Effects of a seed pulse on rogue-wave formation for midinfrared supercontinuum generation in chalcogenide photonic crystal fibers

Saili Zhao,[1,2,*] Hua Yang,[1,3,†] and Yuzhe Xiao[4,‡]

[1]*Key Laboratory for Micro/Nano Optoelectronic Devices of Ministry of Education, College of Computer Science and Electronic Engineering, Hunan University, Changsha 410082, China*

[2]*Electrical Engineering Department, University of California, Los Angeles, California 90095, USA*

[3]*Synergetic Innovation Center for Quantum Effects and Application, Hunan Normal University, Changsha 410082, China*

[4]*Department of Electrical Engineering, University of Wisconsin–Madison, Madison, Wisconsin 53715, USA*

(Received 3 August 2018; published 9 October 2018)

We numerically study the characteristics of optical rogue waves (RWs) in midinfrared supercontinuum (MIR-SC) generation with a femtosecond pump in the anomalous dispersion regime of a chalcogenide photonic crystal fiber. An approach based on seed-induced modulation instability is used to regulate the formation of optical RWs. By carrying out multiple simulations in the presence of noise, we show that optical RWs can be generated in a more controlled manner by providing a seed with an optimum modulation frequency. The redshift range of optical RWs is expanded to a considerable extent in the seed-induced case rather than the noise-induced case. Furthermore, the increase of pump power can facilitate the redshift of optical RWs. These results demonstrate how a seed pulse affects the formation of optical RW for MIR-SC generation with a femtosecond pump in the anomalous dispersion regime of fiber, indicating that optical RW can be used to generate ultra-broadband MIR-SC.

DOI: 10.1103/PhysRevA.98.043817

I. INTRODUCTION

Supercontinuum (SC) sources based on optical fibers have drawn extensive attention in the past decades [1]. Especially, expanding the wavelength range of the SC towards the midinfrared (MIR) regime has been an active field of research owing to its potential applications in biomedical sensing, optical tomography, metrology, microscopy, and spectroscopy [2–4]. Photonic crystal fiber (PCF) is a great boost to the development of SC generation because of its high nonlinearity, low confinement loss, and tunable chromatic dispersion [5]. Previous work on SC generation mainly focused on silica PCFs, which are not very suitable for MIR-SC generation due to high absorption of silica in this spectral range [1,6,7]. With the wider transmission window into long-wavelength range and higher nonlinearity, chalcogenide PCFs have been studied as excellent candidates for MIR-SC generation [8–10].

Dispersion engineering of chalcogenide fibers is very important because bulk chalcogenide glass usually suffers from large normal dispersion in the infrared regime, which dramatically reduces the efficiency of spectral expansion [11]. Several research groups have proposed specifically designed chalcogenide PCFs, which are pumped in the anomalous dispersion regime to generate broadband MIR-SC [9–14]. For instance, Hu *et al.* introduced a procedure for maximizing the bandwidth of the SC spectrum in arsenic-selenide (As_2Se_3) chalcogenide PCFs with a hexagonal geometry [12] and Ahmad *et al.* showed that a chalcogenide PCF with a circular lattice is suitable for ultrawideband MIR-SC generation [13]. Therefore, it is achievable to obtain an efficient and broadband MIR-SC generation by regulating the geometry structure of a chalcogenide PCF.

Recently, there has been a growing interest in the stability of light source and noise properties in the field of optical fiber SC generation [1,14]. For SC generation pumped by long pulse (picosecond and longer), the underlying spectral broadening mechanisms and noise properties have been well studied [15–18]. In 2007, Solli *et al.* have shown that the shot-to-shot statistics of broadband SC spectra are associated with the excitation of statistically rare rogue soliton events [15]. Subsequently, widespread attention has been paid to manipulate and harness the optical rogue wave (RW). Several approaches have been proposed for manipulation of RWs generated by a long pump, including triggering the continuous wave [19,20], utilizing a sliding frequency [21,22], and seeding a coherent pulse [23,24]. However, there are only a couple of studies on the formation and control of optical RWs with a femtosecond-long pump in the normal dispersion regime [25,26]. Since modulation instability (MI) and soliton-related dynamics are completely inhibited in the normal dispersion region, SC spectral width is much smaller compared with that pumped in the anomalous dispersion region [1]. Moreover, the majority of previous studies on optical RWs focused on the spectral range from visible to near-infrared [27–29], but quite limited in the MIR range [30]. The optical RW is featured as the statistically rare event associated with extreme redshift and high-intensity long-wavelength Raman soliton pulse [15–17],

*zhaosaili@hnu.edu.cn

†Corresponding author: huayang@hnu.edu.cn

‡xiao5@wisc. edu

and hence active manipulation is beneficial to the expansion of bandwidth and an increase of conversion efficiency towards MIR wavelength. Also, pumping with a femtosecond pulse can transfer more energy away from the pump and further decrease the amount of residual pump, generating a flatter MIR-SC spectrum [1,31]. Therefore, effective control of optical RW formation can lead to a much broader and smoother MIR-SC spectrum when pumping a femtosecond pulse in the anomalous dispersion regime of a chalcogenide PCF.

In this paper, the As_2Se_3 chalcogenide PCF is used as the propagation medium to generate the MIR-SC by pumping a femtosecond pulse in the anomalous dispersion regime close to the fiber zero-dispersion wavelength (ZDW). Based on multiple simulations, we present the effects of a seed pulse on optical RW formation for MIR-SC generation in chalcogenide PCFs. Induced MI can suppress the noise effect and thereby control the behavior of optical RWs within a certain range in the femtosecond regime. By measuring the statistic properties of MIR-SC spectra, we show that not only the bandwidth but also the stability of the MIR-SC can be improved by providing an optimum seed.

II. PROPAGATION MODEL AND MODULATION INSTABILITY GAIN

A. Propagation model in chalcogenide PCFs

MIR-SC generation in chalcogenide PCFs can be modeled by the following generalized nonlinear Schrödinger equation (GNLSE) [1,31]:

$$\frac{\partial A}{\partial z}+\frac{a}{2}A-\sum_{k\geqslant 2}\frac{i^{k+1}\beta_k}{k!}\frac{\partial^k A}{\partial T^k}=i\gamma\left(1+i\tau_{\text{shock}}\frac{\partial}{\partial T}\right)\times\left\{A(z,T)\left[\int_{-\infty}^{+\infty}R(T')|A(z,T-T')|^2dT'+i\Gamma_R(z,T)\right]\right\}, \tag{1}$$

where $A(z,T)$ is the field envelope. The left-hand side of Eq. (1) models linear propagation effects, with a as the linear loss coefficient and the β_k's as dispersion coefficients for different orders. The right-hand side models nonlinear effects with γ as nonlinear coefficient. The response function $R(t)=f_R h_R(t)+(1-f_R)\delta(t)$ includes both delayed Raman and instantaneous electronic contribution, with f_R as the fractional contribution of Raman response and $h_R(t)=(\tau_1^{-1}+\tau_2^{-2}\tau_1)\exp(-t/\tau_2)\sin(t/\tau_1)$ as the Raman response function with Raman period (τ_1) and lifetime (τ_2). The time derivation term on the right-hand side models the dispersion of the nonlinearity, characterized by a time constant τ_{shock}. Noise is included in the frequency domain through a one-photon-per-mode background, and via the term Γ_R which describes thermally driven spontaneous Raman scattering [1,18].

We consider a Gaussian pump pulse ($T_0=200$ fs, $\lambda_0=2500$ nm) and a seed pulse with the following form propagating in a chalcogenide PCF:

$$A(0,T)=\sqrt{P_p}[1+a_0\exp(i2\pi f_{\text{mod}})]\exp\left(-T^2/2T_0^2\right). \tag{2}$$

The peak power of the pump P_p is chosen to be 100 W, while that of the seed is defined as $a_0^2P_p$, where a_0 is the modulation depth. The seed temporally overlaps with the pump, and has a frequency offset f_{mod} with respect to the pump.

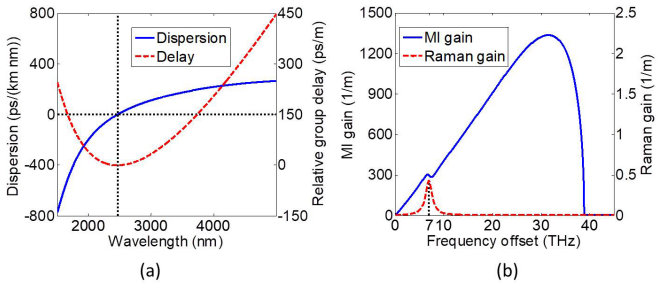

FIG. 1. (a) The dispersion (blue solid curve) and group delay (red dashed curve) profiles of the chalcogenide PCF as a function of wavelength. The vertical dotted line indicates the ZDW at 2466 nm. (b) MI gain (blue solid curve) and Raman gain (red dashed curve) spectra of the chalcogenide PCF as a function of seed frequency offset. The vertical dotted line indicates the Raman gain peak at 7 THz.

The chalcogenide PCF owns a four-circular-ring structure with the same air-hole filling fraction ratio in all rings, the structure and properties of which are identical with that in Ref. [13]. The related structure parameters are as follows: the pitch of the lattice $\Lambda=1.9\,\mu$m, the diameter of each air hole $d=1.3\,\mu$m, and core diameter $2(\Lambda-d/2)=2.5\,\mu$m. By an efficient finite element method, the dispersion curve of the chalcogenide PCF is obtained with a ZDW of 2466 nm, as shown in Fig. 1(a). With 2500 nm as the pump wavelength, we can obtain the related dispersion coefficient values of the Taylor expansion up to the tenth order, as follows: $\beta_2=-0.0313\,\text{ps}^2/\text{m}$, $\beta_3=3.08\times10^{-3}\,\text{ps}^3/\text{m}$, $\beta_4=-1.06\times10^{-5}\,\text{ps}^4/\text{m}$, $\beta_5=7.17\times10^{-8}\,\text{ps}^5/\text{m}$, $\beta_6=-5.3\times10^{-10}\,\text{ps}^6/\text{m}$, $\beta_7=4.80\times10^{-12}\,\text{ps}^7/\text{m}$, $\beta_8=-3.7253\times10^{-14}\,\text{ps}^8/\text{m}$, $\beta_9=1.1885\times10^{-16}\,\text{ps}^9/\text{m}$, $\beta_{10}=1.0076\times10^{-17}\,\text{ps}^{10}/\text{m}$. The group delay curve of the chalcogenide PCF is also illustrated in Fig. 1(a). The nonlinear coefficient γ at the pump wavelength is $14\,923\,\text{W}^{-1}\,\text{km}^{-1}$, a relatively high nonlinearity that helps to broaden the SC spectrum in the MIR regime.

B. Modulation instability gain and Raman gain

During the propagation of a femtosecond pulse, a weak MI perturbation, even though it is only significant in the initial stage, can have a dramatic impact on the generation of optical RWs [26]. To have a close look at the impact of induced MI on the optical pulse, the nonlinear response function and dispersion profile are taken into account to obtain the MI gain spectrum $g(\Omega)$ [1,2]:

$$g(\Omega)=Im\left\{\Delta k_o\pm\sqrt{\Delta k_e+2\gamma P_{\text{p}}\tilde{R}(\Omega)\Delta k_e}\right\}, \tag{3}$$

where Ω is the modulation frequency, and Δk_o and Δk_e are sums over odd- and even-order derivatives of propagation constant β [1,24,31]. $\tilde{R}(\Omega)$ is the Raman response function in frequency, which can be obtained by taking the Fourier

transform of $R(t)$ [31]:

$$\tilde{R}(\Omega) = (1 - f_R) + f_R \frac{\tau_1^2 + \tau_2^2}{\tau_2^2 - \tau_1^2 (i + \tau_2 \Omega)^2}. \quad (4)$$

The material parameters (f_R, τ_1, τ_2) are 0.100, 23.1 fs, and 195.0 fs, respectively [13]. Figure 1(b) plots together the MI gain and Raman gain as a function of modulation frequency at pump power. As shown in Fig. 1(b), the Raman gain peak is located at the frequency offset of 7 THz. For femtosecond pulses, soliton-related dynamics play an important role in the MIR-SC generation, which is closely related to Raman effects [1,31]. Therefore, 7 THz is chosen as the modulation frequency to yield the richest dynamics. In addition, Sørensen *et al.* have proved that modulation frequency located at the Raman gain peak is also beneficial to the improvement of spectral stability [24].

III. NUMERICAL SIMULATIONS IN CHALCOGENIDE PCFs

To see how one can regulate RW formation for MIR-SC generation in the femtosecond regime, we numerically simulate the propagation of a pump pulse with a seed in a 6-cm-long chalcogenide PCF. In this section, we compare the MIR-SC generated by the unseeded pump with that by the seeded pump, both in the presence of random noise. In order to isolate the effect of noise, the initial random noise seed is fixed. In this simulation, the soliton order is chosen to be $N = \sqrt{L_D/L_{NL}} = \sqrt{\gamma P_P T_0^2/|\beta_2|} \approx 44$, where $L_D = T_0^2/|\beta_2|$ and $L_{NL} = 1/\gamma P_p$ are the characteristic dispersive and nonlinear length, respectively. A higher-order soliton is a particular class of solution of GNLSE representing a bound state of N fundamental solitons. During the soliton fission process, the injected pulse with sufficient peak power breaks up into a train of individual subpulses in the anomalous dispersion regime. Each of these subpulses is, in fact, a constituent fundamental soliton and the number of subpulses is equal to the incident soliton order N. For a large input pulse width $T_0 = 200$ fs, initial spectral broadening is usefully described in terms of MI process. In this case, the breakup of the pulse temporal envelope into subpulses arises from MI effects, and the fact that this is seeded from noise has dramatic consequences for the SC spectrum, resulting in significant shot-to-shot variation in both temporal and spectral domains. MI can amplify low-level noise at the input, resulting in large fluctuations in the amplitude (and duration) of subsequently generated fundamental solitons. These fluctuations are then converted into wavelength fluctuations through the soliton self-frequency shift, which in turn leads to significant temporal jitter through the dispersion effect. All the intensity plots use the same logarithmic density scale in order to better analyze the pulse evolution under different conditions.

A. Single shot dynamics without seed

Figure 2 illustrates the generation of the RW and SC in the absence of seed ($a_0 = 0$). In this case, noise acts as the input seed, amplified by MI gain. When a femtosecond pulse

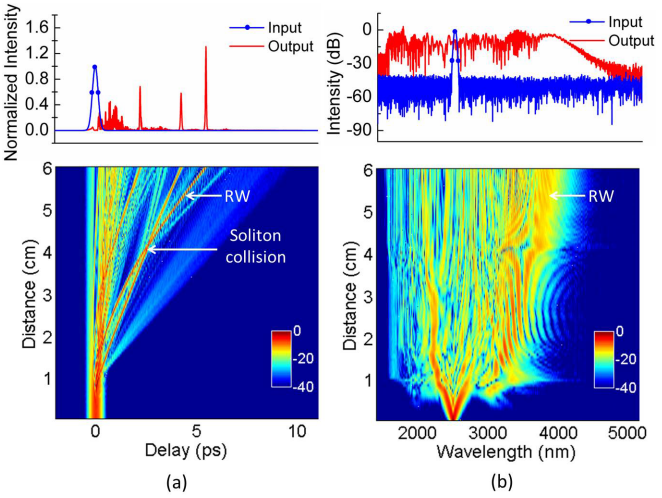

FIG. 2. Single shot simulation of pumping at 2500 nm under the unseeded condition. (a) Input and output pulse shapes (top) and the related temporal evolution (bottom). (b) Input and output spectra (top) and the related spectral evolution (bottom).

is pumped in the anomalous dispersion regime, the signatures of soliton-related dynamics are clear while noise-induced MI effects are less apparent. For given parameters, the calculated MI length ($\sim 16 L_{NL}$, 1.072 cm) is shorter than the calculated characteristic soliton fission length ($\sim L_D/N$, 2.9 cm). Therefore, before higher-order dispersion or Raman scattering becomes significant, noise-induced MI leads to the breakup of higher-order solitons, generating a series of fundamental solitons, as shown in the bottom part of Fig. 2(a) [1,18]. Subsequently, multiple collisions occur between these fundamental solitons due to their differences in group velocities. Significant soliton-collision-induced energy exchange yields a higher-energy RW and a lower-amplitude residual pulse. In addition, the interaction between dispersive waves (DWs) and fundamental solitons is another important mechanism to generate RW. Then the most powerful RW undergoes the strongest Raman self-frequency shift under the Raman effects. As shown in the top part of Fig. 2(a), the RW has a higher intensity and a larger time delay in contrast with other solitons. Figure 2(b) shows that the RW is located at the longest wavelength in the spectral domain. In the initial stage of spectral evolution, spectrum broadening is almost symmetric because of self-phase modulation. When propagation distance increases to 0.3 cm, MI comes into action in the spectral evolution, where a single set of sidebands with weak amplitude is generated at the peaks of the calculated Raman gain spectrum. In this case, noise as a probe is amplified by MI gain, resulting in spectral fluctuations. Even such a small noise-induced MI perturbation plays a vital role in the formation of RWs with extreme redshift. It is obvious that the generation of RWs benefits spectral expansion of the MIR-SC to a wider range. Nevertheless, due to the randomness of noise, the emergence of a RW based on noise-induced MI is a sudden and rare event, which does harm to spectral stability of the MIR-SC (please see discussions on statistic properties in Sec. IV).

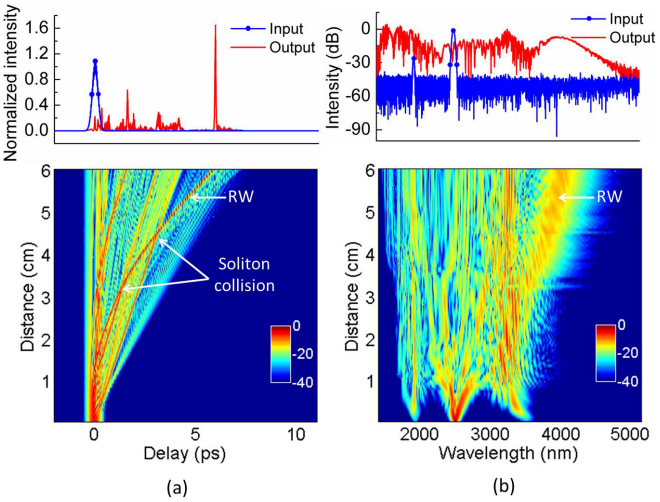

FIG. 3. Single shot simulation of pumping at 2500 nm with a seed of 0.05 modulation depth at the modulation frequency of 7 THz. (a) Input and output pulse shapes (top) and the related temporal evolution (bottom). (b) Input and output spectra (top) and the related spectral evolution (bottom).

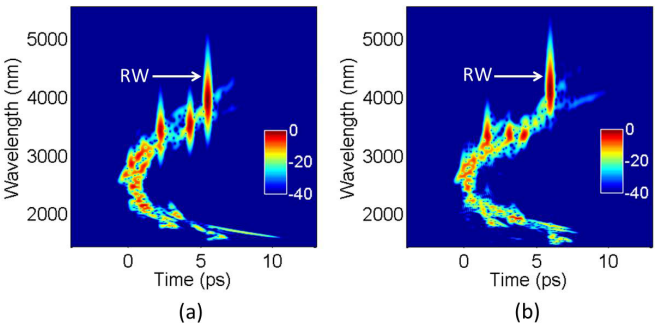

FIG. 4. Output spectrograms (a) without seed and (b) with a seed of 0.05 modulation depth at the modulation frequency of 7 THz, which correspond to Figs. 2 and 3, respectively.

B. Single shot dynamics with seed

Providing a seed with an optimum frequency offset relative to the pump can ensure a deterministic pulse breakup, improve spectral stability of the MIR-SC, and therefore reduce the noise effect. Figure 3 shows that a weak pulse with a modulation depth of 0.05 and a frequency offset of 7 THz relative to the pump is used as the seed. The seed can be observed in the input spectrum shown in the top part of Fig. 3(b). In Fig. 3(a), the breakup of higher-order solitons emerges at a quicker rate compared with that without seed, which indicates a seed can strongly affect MI. This phenomenon can be understood physically because the seed creates an initial modulation on the pump that will see preferential growth relative to the noise [23,24,32]. Subsequently, a train of fundamental solitons are split out due to the seed-induced MI. These fundamental solitons in Fig. 3(a) are ejected earlier than those in Fig. 2(a). Since the peak powers and durations of these fundamental solitons are different, they have different group velocities under the perturbation of higher-order dispersion and Raman scattering along with the propagation [33]. Soon afterwards, multiple collisions between solitons take place, leading to energy exchange between them. Compared with the unseeded case, the number of collisions between fundamental solitons is increased in this seeded case, generating a RW with a higher intensity and a larger redshift. As illustrated in the bottom part of Fig. 3(a), one can see that the output RW goes through two collisions at the propagation distance of 3.2 and 4.5 cm, respectively. In the spectral domain, a single set of sidebands with strong amplitude is generated in the initial stage of MIR-SC generation. Such a strong induced MI perturbation plays a critical role in spectral evolution and RW generation. Next, a clear soliton, namely, the optical RW, is ejected at 3.2 cm and then undergoes continuous shift to longer wavelengths due to Raman self-frequency shift. Since the strong MI process is induced by a specific seed rather than random noise, RWs can be generated in a more controlled manner (please see discussions on statistic properties in Sec. IV). Moreover, the optical RW generated in Fig. 3(b) can redshift to a longer wavelength in contrast with that in Fig. 2(b), which is beneficial to the generation of an ultrabroadband MIR-SC spectrum.

C. Comparison between unseeded and seeded cases

In order to better illustrate the advantages of the seed on RW formation, output spectrograms without and with a seed are plotted in Figs. 4(a) and 4(b), respectively. A significant difference between the two spectrograms is observed at the long-wavelength side, where the number and the intensity of solitons are quite different. The optical RW has a higher intensity and a larger frequency redshift in the seeded case compared with that in the unseeded case. However, the intensities of the other fundamental solitons in the seeded case are lower than those in the unseeded case. The above phenomena result from the differences in the strength of MI sidebands and number of multiple collisions in the two cases. In the noise-induced case, the intensity of MI sidebands is very weak, which leads to a slow breakup of fundamental solitons. Such a phenomenon reduces the strength of collisions and the rate of frequency redshift, resulting in a low-efficiency energy exchange between solitons, while providing a seed with 7-THz modulation frequency can make the MI sidebands with a much higher intensity generated at a quicker rate, resulting in a faster breakup of the temporal pulse. Such a phenomenon contributes to the emergence of multiple collisions, and thereby generates a RW with a higher intensity and a larger redshift. When a series of fundamental solitons are ejected in the anomalous dispersion regime, DWs are radiated in the normal dispersion regime from the pump. When the group-velocity matching condition between the solitons and DWs is met, solitons on the long-wavelength side interact through cross-phase modulation with the DWs on the short-wavelength side, which can lead to soliton trapping phenomena [1,31]. In this case, spectral locations of the DWs are related to those of the solitons. Because the RW in Fig. 4(b) has a larger frequency redshift compared with that in Fig. 4(a), the corresponding trapped DWs can obtain a larger frequency blueshift, which is beneficial to spectral expansion.

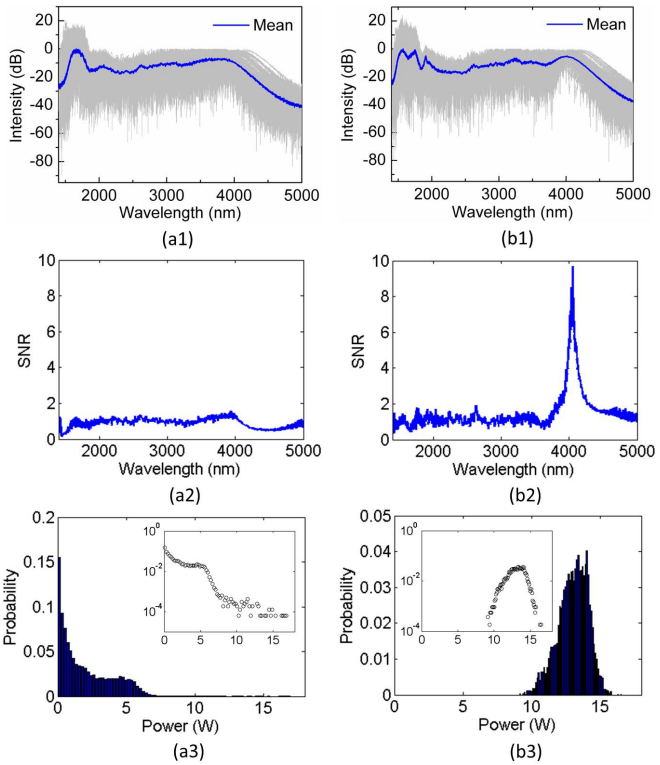

FIG. 5. The comparison between (a1, a2, a3) noise- and (b1, b2, b3) seed-induced MIR-SC generation with 0.05 modulation depth at the modulation frequency of 7 THz. (a1, b1) Output spectral characteristics with 100 individual simulations (gray lines) and the calculated mean spectrum (blue line). (a2, b2) SNR. (a3, b3) Peak power histograms when filtering above 3800 nm (the inset presents the corresponding histograms in log-log scale).

IV. STATISTICAL PROPERTIES OF THE RW AND MIR-SC

To examine the spectral stability of the MIR-SC in the femtosecond regime, multiple simulations are carried out in the presence of different random noise, resulting in spectral and temporal structures with shot-to-shot fluctuations. In this section, statistical properties of the RW and MIR-SC are investigated using an ensemble of 100 realizations.

Figure 5 shows the comparisons between noise- and seed-induced MIR-SC generation when a femtosecond pulse is pumped in a chalcogenide PCF. Figures 5(a1) and 5(b1) compare the output MIR-SC spectral characteristics, where gray lines represent an ensemble of 100 individual simulations with random noise and the blue line represents the calculated mean from the ensemble. In contrast with Fig. 5(b1), Fig. 5(a1) shows more significant shot-to-shot fluctuations in the spectral intensities around 4000 nm. Such instability results from the significant shot-to-shot differences in Raman soliton dynamics and frequency brought by the random nature of noise-induced MI [16–18] while in Fig. 5(b1) providing a seed leads to considerably different spectral characteristics. First, an increased overall bandwidth with extended long-wavelength edge is observed in the seed-induced case. Such a phenomenon is expected since seed-induced MI facilitates the initiation of soliton fission and the emergence of multiple collisions, which further expand the MIR-SC spectrum. In addition, the peak power is enhanced at the long wavelength while reduced at the pump due to the same reason. At last, a well-isolated RW shows up at the long-wavelength edge. This is because the optical RW is generated in a more deterministic manner with a seed.

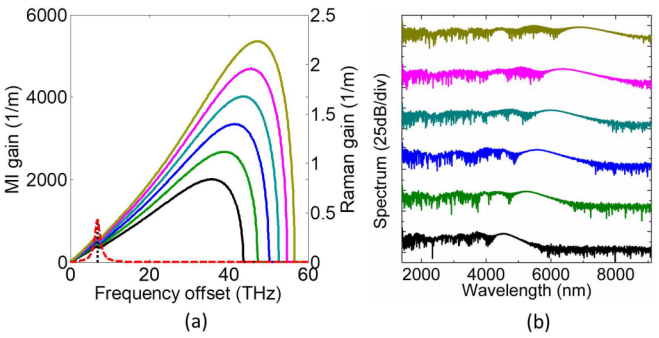

FIG. 6. (a) Raman gain spectrum (red dashed curve) and MI gain spectra with different pump peak power as a function of seed frequency offset. The dotted line is located at the Raman gain peak at 7 THz. (b) Calculated average spectra from 100 simulations with different pump peak power. The peak power of the pump changes in steps of 50 W from 150 to 400 W (from bottom to top).

The intensity stability can be further quantified by the signal-to-noise ratio (SNR), which is defined as the ratio of the mean to the standard deviation [24,26]. Figures 5(a2) and 5(b2) show the comparison of SNR between the noise- and seed-induced MIR-SC generation. In Fig. 5(a2), a low flat SNR is observed over the entire spectral bandwidth except that with a tiny projection at the long wavelength. The tiny projection around 4000 nm shows the emergence of the optical RW at a low probability. In contrast, providing a seed can pull the projection to a longer wavelength and a higher value, as shown in Fig. 5(b2). In order to further present the remarkable improvement in spectral stability, Figs. 5(a3) and 5(b3) compare the histograms of peak power probability distribution at the long wavelength in the noise- and seed-induced case. In order to isolate the shot-to-shot fluctuations in the long-wavelength edge of the MIR-SC, a long-pass filter is used to select the spectrum components above a certain wavelength. Here we use a filter with 3800-nm cutoff wavelength that selects the −20-dB long-wavelength edge of MIR-SC spectra. In Fig. 5(a3), the histogram demonstrates a typical heavy-tailed "L-shaped" probability distribution, which characterizes the emergence of the optical RW as a high-amplitude event with a low probability in the unseeded case [15,23]. After adding a weak pulse with an optimum modulation frequency as the seed, a distinctly localized Gaussian-like distribution is observed in Fig. 5(b3) due to the generation of the optical RW at a high probability, indicating an enhanced spectral stability [25,26].

Figure 6 shows the effect of pump peak power on optical RW formation in the femtosecond regime. As shown in Fig. 6(a), even though the peak of the MI gain spectrum gradually shifts to a longer wavelength with the increase of pump power [Eq. (3)], the Raman gain spectrum does not change [Eq. (4)]. Because a seed at the Raman gain peak can efficiently enhance the spectral stability, 7 THz is still chosen as the modulation frequency of the seed. Figure 6(b)

shows the calculated average spectra from 100 simulations under different pump peak power. As shown here, the optical RW experiences a redshift in central frequency accompanied by an increase in the spectral bandwidth as the pump power increases. Such a phenomenon is expected since the increase of pump power generates more fundamental solitons, which further accelerates the emergence of multiple collisions as well as the redshift of Raman solitons. Therefore, increasing the pump power can help to expand the MIR-SC bandwidth based on the effects of a seed pulse on optical RW formation.

V. CONCLUSIONS

In this paper, we present a mechanism to generate broader and more stable MIR-SC generation based on the effects of a seed pulse on optical RW formation when pumping a femtosecond pulse in the anomalous dispersion regime of a chalcogenide PCF. These results indicate that providing a seed with an optimum modulation frequency can dramatically enhance the spectral stability by generating the optical RW in a more controlled manner. In addition, the frequency of the optical RW can redshift to a longer wavelength based on the seed-induced MI, which contributes to spectral expansion. At last, the increase of pump power can also accelerate the redshift of the RW, and further expand the spectral bandwidth. We believe the results of this paper will give insight on the impact of a seed on RW generation, which can further promote the application of the MIR-SC in practice.

ACKNOWLEDGMENTS

This work was supported by the National Natural Science Foundation of China (Grant No. 61275137), Natural Science of Hunan province of China (Grant No. 2018JJ2061), and China Scholarship Council.

[1] J. M. Dudley, G. Genty, and S. Coen, Rev. Mod. Phys. **78**, 1135 (2006).
[2] A. Schliesser, N. Picqué, and T. W. Hänsch, Nature Photon. **6**, 440 (2012).
[3] J. Swiderski and M. Michalska, Opt. Lett. **39**, 910 (2014).
[4] S. Dupont, C. Petersen, J. Thøgersen, C. Agger, O. Bang, and S. R. Keiding, Opt. Express **20**, 4887 (2012).
[5] J. C. Knight, Nature (London) **424**, 847 (2003).
[6] S. Zhao, H. Yang, N. Chen, X. Fu, and C. Zhao, IEEE Photonics J. **7**, 7102709 (2015).
[7] I. A. Sukhoivanov, S. O. Lakushev, O. V. Shulika, J. A. Andrade-Lucio, A. Díez, and M. Andrés, Opt. Express **22**, 30234 (2014).
[8] B. J. Eggleton, B. Luther-Davies, and K. Richardson, Nature Photon. **5**, 141 (2011).
[9] C. R. Petersen, U. Møller, I. Kubat, B. Zhou, S. Dupont, J. Ramsay, T. Benson, S. Sujecki, N. Abdel-Moneim, Z. Tang, D. Furniss, A. Seddon, and O. Bang, Nature Photon. **8**, 830 (2014).
[10] R. A. H. Ali, M. F. O. Hameed, and S. S. A. Obayya, J. Lightw. Technol. **34**, 5423 (2016).
[11] P. Zhang, P. Yang, X. Wang, R. Wang, S. Dai, and Q. Nie, Opt. Express **24**, 28400 (2016).
[12] J. Hu, C. R. Menyuk, L. B. Shaw, J. S. Sanghera, and I. D. Aggarwal, Opt. Express **18**, 6722 (2010).
[13] R. Ahmad, M. Komanec, and S. Zvanovec, IEEE Photon. Tech. Lett. **28**, 23 (2016).
[14] L. Liu, K. Nigasaka, G. Qin, T. Suzuki, and Y. Ohishi, Appl. Phys. Lett. **108**, 011101 (2016).
[15] D. R. Solli, C. Ropers, P. Koonath, and B. Jalali, Nature (London) **450**, 1054 (2007).
[16] D. R. Solli, G. Herink, B. Jalali, and C. Ropers, Nature Photon. **6**, 463 (2012).
[17] J. M. Dudley, F. Dias, M. Erkintalo, and G. Genty, Nature Photon. **8**, 755 (2014).
[18] G. Genty, J. Dudley, and B. Eggleton, Appl. Phys. B **94**, 187 (2009).
[19] K. K. Y. Cheung, C. Zhang, Y. Zhou, K. K. Y. Wong, and K. K. Tsia, Opt. Lett. **36**, 160 (2011).
[20] Q. Li, F. Li, K. K. Y. Wong, A. P. T. Lau, K. K. Tsia, and P. K. A. Wai, Opt. Express **19**, 13757 (2011).
[21] D. R. Solli, C. Ropers, and B. Jalali, Phys. Rev. Lett. **101**, 233902 (2008).
[22] J. M. Dudley, G. Genty, and B. J. Eggleton, Opt. Express **16**, 3644 (2008).
[23] S. Zhao, H. Yang, N. Chen, and C. Zhao, Sci. Rep. **7**, 39926 (2017).
[24] S. T. Sørensen, C. Larsen, U. Møller, P. Mselund, C. L. Thomsen, and O. Bang, J. Opt. Soc. Am. B **29**, 2875 (2012).
[25] M. Erkintalo, G. Genty, and J. M. Dudley, Opt. Lett. **14**, 2468 (2009).
[26] Q. Li and X. Duan, Opt. Express **23**, 16364 (2015).
[27] S. Zhao, H. Yang, C. Zhao, and Y. Xiao, Opt. Express **25**, 7192 (2017).
[28] A. Demircan, S. Amiranashvili, C. Bree, C. Mahnke, F. Mitschke, and G. Steinmeyer, Sci. Rep. **2**, 850 (2012).
[29] K. Hammani, C. Finot, J. M. Dudley, and G. Millot, Opt. Express **16**, 16467 (2008).
[30] S. M. Hernandez, P. I. Fierens, J. Bonetti, and D. F. Grose, arXiv:1605.03144.
[31] G. P. Agrawal, *Nonlinear Fiber Optics* (Academic, New York, 2012).
[32] D. M. Nguyen, T. Godin, S. Toenger, Y. Combes, B. Wetzel, T. Sylvestre, J. Merolla, L. Larger, G. Genty, F. Dias, and J. M. Dudley, Opt. Lett. **38**, 5338 (2013).
[33] A. Armaroli, C. Conti, and F. Biancalana, Optica **2**, 497 (2015).